Korean J. Chem. Eng., 35(2), 364-374 (2018)
DOI: 10.1007/s11814-017-0271-2

pISSN: 0256-1115
eISSN: 1975-7220

Double diffusive effects on radial fingering in a porous medium or a Hele-Shaw cell

Min Chan Kim†

Department of Chemical Engineering, Jeju National University, Jeju 63243, Korea
(*Received 11 August 2017 • accepted 25 September 2017*)

Abstract−Double diffusive effects on the growth of radial viscous fingering in a porous medium or a Hele-Shaw cell were analyzed theoretically. Under linear stability theory, the stability equations were derived in a self-similar domain. The stability equations were transformed using the normal mode analysis and solved analytically and numerically. Regardless of the diffusivity ratio, Le, the Péclet number, Pe, makes the system unstable, i.e., accelerates the growth of instabilities. The double diffusive effects on the growth of the instabilities were strongly dependent on the viscosity distribution. If the displaced phase has stable viscosity distribution, as Le increases, the system becomes unstable regardless of the magnitude of Pe. However, as Le increases, the growth of the instabilities is suppressed if the displaced phase has unstable viscosity distribution.

Keywords: Viscous Fingering, Radial Flow, Double Diffusion, Hele-Shaw Cell, Porous Medium

INTRODUCTION

Miscible viscous fingering, occurring in a porous medium when a fluid of a given viscosity displaces another miscible more viscous fluid, was first studied experimentally by Hill [1]. This fingering instability has been the focus of numerous works devoted to studying enhanced oil recovery, pollution spreading in soils or efficient chromatographic column design, and so on [2-7]. Recently, De Wit et al. [8-12] analyzed the precipitation patterns in a radial Hele-Shaw cell experimentally. In their precipitation reactions, one reactant was injected radially into another ambient reactant. If the injecting solution is less viscous than the ambient displaced one, miscible viscous fingering can be onset and this fingering motion can be visualized through the precipitation patterns. In these precipitation systems, because the viscosity distributions are determined by the diffusivity ratio and the chemical reaction rate, the double diffusive effects cannot be avoidable. Brau et al. [13] theoretically and experimentally considered the properties of reaction-diffusion-advection fronts of A+B→C reaction in a radial geometry. However, the double diffusive effects on the miscible viscous fingering in radial flows have been less focused than in rectilinear systems [14-16].

The viscous fingering occurring in radial source flows has attracted many researchers' interest (see Tan and Homsy [17], Yortsos [18] and the references given therein). Later, Riaz and Meiburg [19,20] and Riaz et al. [21] extended this problem by considering various effects such as 3-dimensional disturbances, velocity-induced dispersion and concentration-dependent diffusion. They solved the stability problem with linear stability theory and direct numerical simulation. If the viscosity differences between miscible fluids can be related to temperature and/or composition changes, the two different components' diffusion at different rates affects the onset and growth of the viscous fingering, and studies of such viscous fingering can be performed by analyzing displacements between two miscible solutions at different temperatures or containing a viscosity changing solute in variable concentration. Pritchard [22] revisited this problem by considering double diffusive effects due to the heat and mass transfer.

We analyzed the effect of two different components diffusion at different rates on the onset and growth of the viscous fingering the radial source flow under linear theory. Under the normal mode analysis, linear stability equations were derived and solved analytically by using the spectral method and numerically by numerical shooting method. From the linear stability results, the onset conditions and the growth of the azimuthal instability were predicted.

GOVERNING EQUATIONS AND BASE FIELDS

The two-dimensional flow that results from the injection of fluid

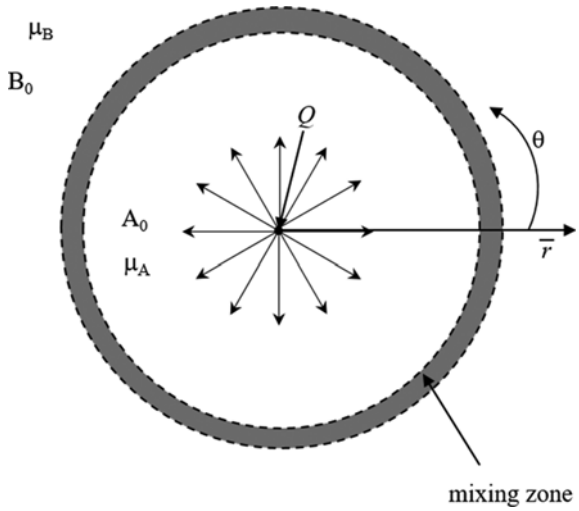

Fig. 1. Schematic diagram of system considered here.

†To whom correspondence should be addressed.
E-mail: mckim@jejunu.ac.kr

into a horizontal porous layer or a Hele-Shaw cell, whose permeability is K, from a line source at position $\bar{r}=0$ with a constant areal flux Q is considered here. The solute compositions of the injected and ambient fluids are A_0 and B_0, respectively. Fig. 1 illustrates the present system schematically. By neglecting the mechanical dispersion, the dimensionless governing equation in the polar coordinate can be written as [17,22],

$$\frac{1}{r}\frac{\partial}{\partial r}(ru)+\frac{1}{r}\frac{\partial v}{\partial\theta}=0, \tag{1}$$

$$\frac{\partial p}{\partial r}=-\mu u, \tag{2}$$

$$\frac{1}{r}\frac{\partial p}{\partial\theta}=-\mu v, \tag{3}$$

$$\frac{\partial a}{\partial\tau}+\left\{\frac{1}{r}\frac{\partial(rua)}{\partial r}+\frac{1}{r}\frac{\partial(va)}{\partial\theta}\right\}=\frac{1}{Pe}\left\{\frac{1}{r}\frac{\partial}{\partial r}\left(r\frac{\partial a}{\partial r}\right)+\frac{1}{r^2}\frac{\partial^2 a}{\partial\theta^2}\right\}, \tag{4}$$

$$\frac{\partial b}{\partial\tau}+\left\{\frac{1}{r}\frac{\partial(rub)}{\partial r}+\frac{1}{r}\frac{\partial(vb)}{\partial\theta}\right\}=\frac{Le}{Pe}\left\{\frac{1}{r}\frac{\partial}{\partial r}\left(r\frac{\partial b}{\partial r}\right)+\frac{1}{r^2}\frac{\partial^2 b}{\partial\theta^2}\right\}. \tag{5}$$

where the azimuthal coordinate is denoted by θ. Here, u, v, a and b are the dimensionless velocities in the (r, θ)-directions, and the dimensionless concentrations of the solute A and B, respectively. We introduced $\sqrt{K}$, K/Q, Q/$\sqrt{K}$, μ_0, μ_0Q/K, A_0 and B_0 used as length, time, velocity, viscosity, pressure, concentrations A and concentration B scales, respectively, where μ_0 is the viscosity of the common solvent. The important parameters to govern the present system are the Péclet number, Pe, and the Lewis number, Le, defined as [22]

$$Pe=\frac{Q}{D_A}\text{ and }Le=\frac{D_B}{D_A}, \tag{6}$$

where D_i is the effective diffusivity of the solute i(=A or B), rather than the molecular diffusivities. Because the diffusivities in a porous medium are smaller than the molecular diffusivities in a homogeneous medium, the effective diffusivities are proposed considering the average cross-sectional area open to diffusion and the distance traveled by molecules in a porous medium. The Péclet number means the ratio of the convective transfer rate and diffusive one. It is well-known that the diffusive term makes the convective motion stable, which will be discussed later, and therefore, higher values of the Péclet number promote instability.

Following the previous studies [14-16,22], the viscosity is assumed to depend exponentially on the concentrations of A and B as

$$\mu=\mu_0\exp(-R_A a-R_B b), \tag{7}$$

where R_A and R_B are defined as

$$R_A=-\frac{d\ln\mu}{da}\text{ and }R_B=-\frac{d\ln\mu}{db}. \tag{8}$$

Since viscous fingering is driven by viscosity mismatch which is quantified by (R_A-R_B), the fingering instability can never be expected for $(R_A-R_B)=0$. However, even though there is a significant viscosity mismatch, the system can remain stable if there is no flow: Pe=0. This means that the stability of the present system is controlled by both Pe and (R_A-R_B) not Pe or (R_A-R_B) alone.

Before the onset of fingering motion, the base concentration field is governed by

$$\frac{\partial a_0}{\partial\tau}+\frac{1}{r}\frac{\partial a_0}{\partial r}\left(1-\frac{1}{Pe}\right)=\frac{1}{Pe}\frac{\partial^2 a_0}{\partial r^2}, \tag{9}$$

$$\frac{\partial b_0}{\partial\tau}+\frac{1}{r}\frac{\partial b_0}{\partial r}\left(1-\frac{Le}{Pe}\right)=\frac{Le}{Pe}\frac{\partial^2 b_0}{\partial r^2}, \tag{10}$$

under the following boundary conditions:

$$a_0=1\text{ and }b_0=0\text{ at }r=0, \tag{11a}$$

$$b_0=0\text{ and }b_0=1\text{ as }r\to\infty. \tag{11b}$$

The solutions of the above equations are

$$a_0(\xi)=\frac{\Gamma((Pe/2),\,\xi)}{\Gamma(Pe/2)}, \tag{12a}$$

$$b_0(\xi)=\frac{\gamma(Pe_L/2,\,\xi_L)}{\Gamma(Pe_L/2)}, \tag{12b}$$

where $\xi=Pe\,r^2/(4\tau)$, $Pe_L=Pe/Le$, $\xi_L=\xi/Le$, $\xi=Pe/2$ is the displacing front, and the subscript "0" represents the base quantities. $\Gamma(s)=\int_0^\infty t^{s-1}\exp(-t)dt$, $\Gamma(s,x)=\int_x^\infty t^{s-1}\exp(-t)dt$ and $\gamma(s,x)=\int_0^x t^{s-1}\exp(-t)dt$ are the gamma function, the upper incomplete gamma function and the lower incomplete gamma function, respectively.

For the limiting case of Pe$\to\infty$, which results in the most unstable scenario, the above concentration fields (12) are reduced as

$$a_0(\eta)=\frac{1}{2}\operatorname{erfc}(\eta), \tag{13a}$$

$$b_0(\eta)=\frac{1}{2}\operatorname{erfc}(-\eta_L), \tag{13b}$$

where $\eta=(\xi-Pe/2)/\sqrt{Pe}$, $\eta_L=\eta/\sqrt{Le}$ and $\eta=0$ is the displacing front.

LINEAR STABILTY ANALYSIS

1. Stability Equations

Under linear theory, the following linear stability equations can be obtained by perturbing Eqs. (1)-(5) [17,22]:

$$\frac{1}{r}\frac{\partial}{\partial r}(ru_1)+\frac{1}{r}\frac{\partial v_1}{\partial\theta}=0, \tag{14}$$

$$\frac{\partial p_1}{\partial r}=-\mu u_1-\left\{\frac{1}{r}\frac{d\mu}{da}a_1+\frac{1}{r}\frac{d\mu}{db}b_1\right\}, \tag{15}$$

$$\frac{1}{r}\frac{\partial p_1}{\partial\theta}=-\mu v_1, \tag{16}$$

$$\frac{\partial a_1}{\partial\tau}+\frac{1}{r}\frac{\partial a_1}{\partial r}+\frac{\partial a_0}{\partial r}u_1=\frac{1}{Pe}\left\{\frac{1}{r}\frac{\partial}{\partial r}\left(r\frac{\partial a_1}{\partial r}\right)+\frac{1}{r^2}\frac{\partial^2 a_1}{\partial\theta^2}\right\}, \tag{17}$$

$$\frac{\partial b_1}{\partial\tau}+\frac{1}{r}\frac{\partial b_1}{\partial r}+\frac{\partial b_0}{\partial r}u_1=\frac{1}{Pe_L}\left\{\frac{1}{r}\frac{\partial}{\partial r}\left(r\frac{\partial b_1}{\partial r}\right)+\frac{1}{r^2}\frac{\partial^2 b_1}{\partial\theta^2}\right\}. \tag{18}$$

The corresponding boundary conditions are

$$ru_1 \to 0,\ a_1 \to 0 \text{ and } b_1 \to 0 \text{ as } r \to 0, \tag{19a}$$

$$u_1 \to 0,\ q_1 \to 0 \text{ and } b_1 \to 0 \text{ as } r \to \infty. \tag{19b}$$

Here the subscripts '0' and '1' mean the base and disturbance quantities, respectively. Eliminating the pressure terms, the linear stability Eqs. (14)-(16) are reduced as

$$\frac{\partial^2(ru_1)}{\partial r^2}+\left(\frac{1}{r}-R_A\frac{\partial a_0}{\partial r}-R_B\frac{\partial b_0}{\partial r}\right)\frac{\partial(ru_1)}{\partial r} + \frac{1}{r^2}\frac{\partial^2}{\partial\theta^2}(ru_1)=R_A\frac{1}{r^2}\frac{\partial^2 a_1}{\partial\theta^2}+R_B\frac{1}{r^2}\frac{\partial^2 b_1}{\partial\theta^2}, \tag{20}$$

Using the similarity variable, $\xi(=\mathrm{Pe}\, r^2/(4\tau))$, Eqs. (17), (18) and (20) are transformed into

$$\xi\frac{\partial^2(ru_1)}{\partial\xi^2}+\left\{1-\left(R_A\frac{da_0}{d\xi}+R_B\frac{db_0}{d\xi}\right)\xi\right\}\frac{\partial(ru_1)}{\partial\xi} + \frac{1}{4\xi}\frac{\partial^2(ru_1)}{\partial\theta^2}=\frac{1}{4\xi}\left\{R_A\frac{\partial^2 a_1}{\partial\theta^2}+R_B\frac{\partial^2 b_1}{\partial\theta^2}\right\}, \tag{21}$$

$$\tau\frac{\partial a_1}{\partial\tau}=\left[\xi\frac{\partial^2}{\partial\xi^2}+\left\{\xi+\left(1-\frac{\mathrm{Pe}}{2}\right)\right\}\frac{\partial}{\partial\xi}+\frac{1}{4\xi}\frac{\partial^2}{\partial\theta^2}\right]a_1-\frac{1}{2}\mathrm{Pe}\frac{da_0}{d\xi}(ru_1), \tag{22}$$

$$\tau\frac{\partial b_1}{\partial\tau}=\mathrm{Le}\left[\xi\frac{\partial^2}{\partial\xi^2}+\left\{\xi_L+\left(1-\frac{\mathrm{Pe}_L}{2}\right)\right\}\frac{\partial}{\partial\xi}+\frac{1}{4\xi}\frac{\partial^2}{\partial\theta^2}\right]b_1 - \frac{1}{2}\mathrm{Pe}_L\frac{db_0}{d\xi_L}(ru_1). \tag{23}$$

Since the coefficients of the above equations are independent of θ under the Fourier mode analysis, the disturbance quantities can be represented as

$$[u_1, a_1, b_1]=[\psi/r, a_1, b_1]\exp(in\theta), \tag{24}$$

where n is the azimuthal wavenumber. Eliminating the pressure terms, the linear stability Eqs. (21)-(23) reduce to

$$\xi\frac{\partial^2\psi}{\partial\xi^2}+\left\{1-\left(R_A\frac{da_0}{d\xi}+R_B\frac{db_0}{d\xi}\right)\xi\right\}\frac{\partial\psi}{\partial\xi}-\frac{n^2}{4\xi}\psi=-\frac{n^2}{4\xi}(R_A a_1+R_B b_1), \tag{25}$$

$$\tau\frac{\partial a_1}{\partial\tau}=\left[\xi\frac{\partial^2}{\partial\xi^2}+\left\{\xi+\left(1-\frac{\mathrm{Pe}}{2}\right)\right\}\frac{\partial}{\partial\xi}-\frac{n^2}{4\xi}\right]a_1-\frac{1}{2}\mathrm{Pe}\frac{da_0}{d\xi}\psi, \tag{26}$$

$$\tau\frac{\partial b_1}{\partial\tau}=\mathrm{Le}\left[\xi\frac{\partial^2}{\partial\xi^2}+\left\{\xi_L+\left(1-\frac{\mathrm{Pe}_L}{2}\right)\right\}\frac{\partial}{\partial\xi}-\frac{n^2}{4\xi}\right]b_1-\frac{\mathrm{Pe}_L}{2}\frac{db_0}{d\xi_L}\psi, \tag{27}$$

The corresponding boundary conditions are

$$a_1 \to 0,\ b_1 \to 0 \text{ and } \psi \to 0 \text{ as } \xi = 0 \text{ and } \xi \to \infty. \tag{28}$$

For the case of large Pe, using $\eta=(\xi-\mathrm{Pe}/2)/\sqrt{\mathrm{Pe}}$, the above stability equations can be approximated as

$$\left\{\frac{\partial^2}{\partial\eta^2}+\left(R_A\frac{da_0}{d\eta}+R_B\frac{db_0}{d\eta}\right)-k^2\right\}\psi^*=-k^2(R_A^* a_1+R_B^* b_1), \tag{29}$$

$$2\tau\frac{\partial a_1}{\partial\tau}=\left\{\frac{\partial^2}{\partial\eta^2}+2\eta\frac{\partial}{\partial\eta}-k^2\right\}a_1-\frac{\partial a_0}{\partial\eta}\psi^*, \tag{30}$$

$$2\tau\frac{\partial b_1}{\partial\tau}=\left\{\frac{\partial^2}{\partial\eta_L^2}+2\eta_L\frac{\partial}{\partial\eta_L}-k_L^2\right\}b_1-\frac{\partial b_0}{\partial\eta_L}\frac{1}{\sqrt{\mathrm{Le}}}\psi^*, \tag{31}$$

where $k=n/\sqrt{\mathrm{Pe}}$, $k_L=k\sqrt{\mathrm{Le}}$ and $R_i^*(=R_i\sqrt{\mathrm{Pe}})$. The proper boundary conditions are

$$\psi \to 0,\ a_1 \to 0 \text{ and } b_1 \to 0 \text{ as } \eta \to \pm\infty. \tag{32}$$

2. Solution Methods

2-1. Spectral Analysis

To analyze Eqs. (25)-(28), according to the Sturm-Liouville theory, let $a_1(\tau, \xi)$ and $b_1(\tau, \xi)$ as

$$a_1(\tau,\xi)=\sum_{m=0}^{\infty}A_m(\tau)\alpha_m\phi_{A,m}(\xi) \quad \text{and} \quad b_1(\tau,\xi)=\sum_{m=0}^{\infty}B_m(\tau)\beta_m\phi_{B,m}(\xi). \tag{33a & b}$$

Here $\phi_{A,m}(\xi)$ and $\phi_{B,m}(\xi)$ are the eigenfunctions of the following Sturm-Liouville equations:

$$L_A\phi_{A,m}=-\lambda_m\phi_{A,m} \text{ and } L_B\phi_{B,m}=-\lambda_m\phi_{B,m}, \tag{34a & b}$$

where $L_A=\left[\xi\frac{d^2}{d\xi^2}+\left\{\xi+\left(1-\frac{\mathrm{Pe}}{2}\right)\right\}\frac{d}{d\xi}\right]$, $L_B=\left[\xi_L\frac{d^2}{d\xi_L^2}+\left\{\xi_L+\left(1-\frac{\mathrm{Pe}_L}{2}\right)\right\}\frac{d}{d\xi_L}\right]$, and λ_m are the eigenvalues corresponding to the eigenfunctions $\phi_{A,m}$ and $\phi_{B,m}$, respectively. It is interesting that the eigenvalues of Eq. (34) are the same if we use ξ and ξ_L in the present analysis. The solutions of the above equations are [22]

$$\phi_{A,m}(\xi)=\exp(-\xi)\xi^{Pe/2}L_m^{Pe/2}(\xi) \text{ and } \phi_{B,m}(\xi)=\exp(-\xi_L)\xi_L^{Pe_L/2}L_m^{Pe_L/2}(\xi_L), \tag{35a & b}$$

and

$$m=(\lambda_m-1)=0, 1, 2, \cdots, \tag{35c}$$

where $L_m^d(\zeta)$ is the associated Laguerre polynomials [23]. The normalization factors α_m and β_m are

$$\alpha_m=\{\Gamma(m+1)/\Gamma(m+Pe/2+1)\}^{-1/2} \text{ and } \beta_m=\{\Gamma(m+1)/\Gamma(m+PeL/2+1)\}^{-1/2}. \tag{36a & b}$$

Therefore, the exact solutions of $a_1(\tau, \xi)$ and $b_1(\tau, \xi)$ can be written as

$$a_1(\tau,\xi)=\exp(-\xi)\xi^{Pe/2}\sum_{m=0}^{\infty}A_m(\tau)\alpha_m L_m^{Pe/2}(\xi) \quad \text{and} \quad b_1(\tau,\xi)=\exp(-\xi_L)\xi_L^{Pe_L/2}\sum_{m=0}^{\infty}B_m(\tau)\beta_m L_m^{Pe_L/2}(\xi_L), \tag{37a & b}$$

It is assumed that $\psi(\xi)$ can be expressed as

$$\psi(\tau,\xi)=n^2\left\{R_A\sum_{m=0}^{\infty}A_m(\tau)\alpha_m\psi_{A,m}(\xi)+R_B\sum_{k=0}^{\infty}B_m(\tau)\beta_m\psi_{B,m}(\xi)\right\}, \tag{38}$$

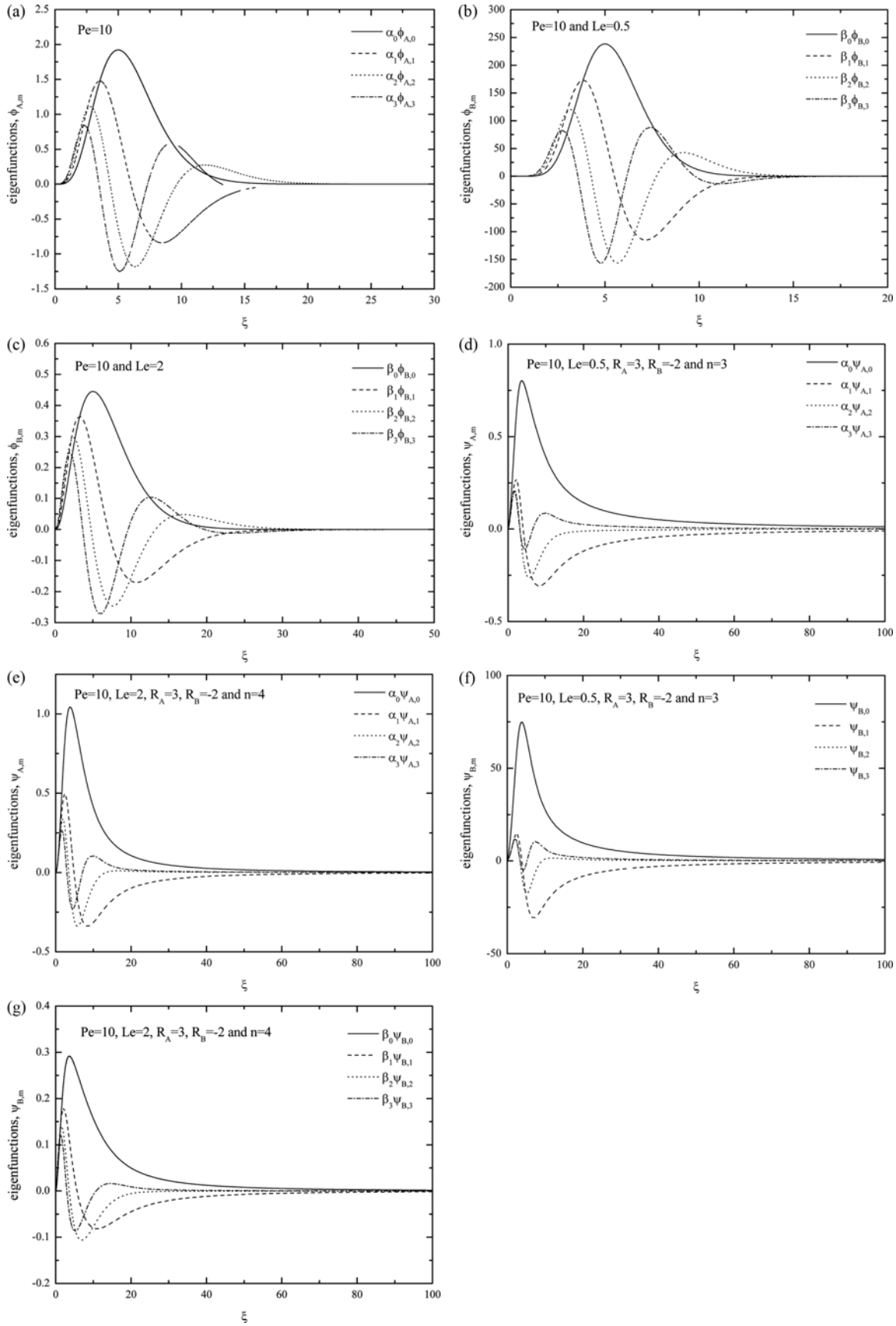

Fig. 2. Eigenfunctions for Pe=10: (a) $\phi_{A,m}(\xi)$, (b) $\phi_{B,m}(\xi)$ for Le=0.5, (c) $\phi_{B,m}(\xi)$ for Le=2, (d) $\psi_{A,m}(\xi)$ for Le=0.5, R_A=3, R_B=−2 and n=4, (e) $\psi_{A,m}(\xi)$ for Le=2, R_A=3, R_B=−2 and n=3, (f) $\psi_{B,m}(\xi)$ for Le=0.5, R_A=3, R_B=−2 and n=4, and (g) $\psi_{B,m}(\xi)$ for Le=2, R_A=3, R_B=−2 and n=3.

where $\psi_{A,m}$ and $\psi_{B,m}$ can be obtained by solving

$$\xi\frac{d^2\psi_{A,m}}{d\xi^2}+\left\{1+\left(R_A\frac{da_0}{d\xi}+R_B\frac{db_0}{d\xi}\right)\xi\right\}\frac{d\psi_{A,m}}{d\xi}-\frac{n^2}{4\xi}\psi_{A,m} =-\frac{1}{4\xi}\exp(-\xi)\xi^{Pe/2}L_m^{Pe/2}(\xi), \tag{39a}$$

$$\xi\frac{d^2\psi_{B,m}}{d\xi^2}+\left\{1+\left(R_A\frac{da_0}{d\xi}+R_B\frac{db_0}{d\xi}\right)\xi\right\}\frac{d\psi_{B,m}}{d\xi}-\frac{n^2}{4\xi}\psi_{B,m} =-\frac{1}{4\xi}\exp(-\xi_L)\xi_L^{Pe_L/2}L_m^{Pe_L/2}(\xi_L). \tag{39b}$$

However, $\psi_{A,m}$ and $\psi_{B,m}$ cannot be expressed in a closed form, and so must be integrated numerically for each set of parameter values. For some example cases, the eigenfunctions $\phi_{A,m}$, $\phi_{B,m}$, $\psi_{A,m}$ and $\psi_{B,m}$ are summarized in Fig. 2.

By substituting $a_1(\tau, \xi)$, $b_1(\tau, \xi)$ and $\psi(\tau, \xi)$ into Eqs. (56) and (57), and using the orthogonality of $L_m^d(\zeta)$'s, Eqs. (26) and (27) can be rewritten in the following matrix form:

$$\frac{d\mathbf{C}}{d\tau}=\mathbf{D}\mathbf{C}, \tag{40a}$$

where

$$\mathbf{C}=\begin{bmatrix}\mathbf{A}\\ \mathbf{B}\end{bmatrix} \text{ and } \mathbf{D}=\begin{bmatrix}\mathbf{D}_{AA} & \mathbf{D}_{AB}\\ \mathbf{D}_{BA} & \mathbf{D}_{BB}\end{bmatrix}, \tag{40b}$$

$$\mathbf{A}=[A_0, A_1, \cdots]^T \text{ and } \mathbf{B}=[B_0, B_1, \cdots]^T. \tag{40c \& d}$$

In principle, **D** is a matrix of infinite rank; however, in practice, we calculate an approximation $\mathbf{D}_N$ of rank 2N+2 by considering only the eigenfunctions $\phi_{A,m}$ and $\phi_{B,m}$ for m=0, 1, ⋯, N. A detailed description for the structure of the matrix **D** is given in the Appendix. Since matrix **D** is independent of τ, the growth rate σ is the maximum eigenvalue of the matrix **D**:

$$\sigma=\max\{\mathrm{eig}(\mathbf{D})\}, \tag{41}$$

where eig(**X**) extracts the eigenvalues of the matrix **X**.

For the case of large Pe and finite R_i, from Eqs. (30) and (31), $a_1(\tau, \eta)$ and $b_1(\tau, \eta)$ can be approximated as

$$a_1(\tau, \eta)=\sum_{m=0}^{\infty}A_m(\tau)\alpha_m\phi_{A,m}(\eta) \text{ and } b_1(\tau, \eta)=\sum_{m=0}^{\infty}B_m(\tau)\beta_m\phi_{B,m}(\eta_L), \tag{42a \& b}$$

where $\phi_{A,m}(\eta)$ and $\phi_{B,m}(\eta)$ are the eigenfunctions of the following Sturm-Liouville equations:

$$\frac{d^2\phi_{A,m}}{\partial\eta^2}+2\eta\frac{d\phi_{A,m}}{d\eta}=-\lambda_m\phi_{A,m} \text{ and } \frac{d^2\phi_{B,m}}{\partial\eta_L^2}+2\eta_L\frac{d\phi_{B,m}}{d\eta_L}=-\lambda_m\phi_{B,m}. \tag{43a \& b}$$

The solutions of the above equations are

$$\phi_{A,m}(\eta)=H_m(\eta)\exp(-\eta^2),\ \phi_{B,m}(\eta)=H_m(\eta_L)\exp(-\eta_L^2) \text{ and } m=(\lambda_m-2)=0, 1, 2, \cdots, \tag{44a, b \& c}$$

where $H_m(\zeta)\left\{=(-1)^m\exp(\zeta^2)\frac{d^m}{d\zeta^m}\exp(-\zeta^2)\right\}$ is the *m*-th degree Hermite polynomial [23]. Therefore, the solution of $a_1(\tau, \eta)$ and $b_1(\tau, \eta)$ can be written as

$$a_1(\tau, \eta)=\exp(-\eta^2)\sum_{m=0}^{\infty}A_m(\tau)\alpha_mH_m(\eta) \text{ and } b_1(\tau, \eta)=\sum_{m=0}^{\infty}B_m(\tau)\beta_m\exp(-\eta_L^2)H_m(\eta_L), \tag{45a \& b}$$

where α_m and β_m can be determined by using the orthogonality of $H_m(\zeta)$'s as

$$\alpha_m=[\sqrt{\pi}\Gamma(m+1)2^m]^{-1/2} \text{ and } \beta_m=[\sqrt{Le\pi}\Gamma(m+1)2^m]^{-1/2}. \tag{46a \& b}$$

Here, we are going to find $\psi^*(\tau, \eta)$ in the following form:

$$\psi^*=(\tau, \eta)=R_A^*\sum_{m=0}^{\infty}A_m(\tau)\alpha_m\psi_{A,m}(\eta) +R_B^*\sum_{m=0}^{\infty}B_m(\tau)\beta_m\psi_{B,m}(\eta), \tag{47a \& b}$$

where $\psi_{A,m}$ and $\psi_{B,m}$ can be obtained by solving

$$\frac{d^2\psi_{A,m}}{d\eta^2}+\left\{\frac{R_A}{\sqrt{\pi}}\exp(-\eta^2)+\frac{R_B}{\sqrt{Le\pi}}\exp(-\eta_L^2)\right\}\frac{d\psi_{A,m}}{d\eta} -k^2\psi_{A,m}=k^2\exp(-\eta^2)H_m(\eta), \tag{48a}$$

$$\frac{d^2\psi_{B,m}}{d\eta_L^2}+\left\{\frac{R_A}{\sqrt{\pi}}\exp(-\eta^2)+\frac{R_B}{\sqrt{Le\pi}}\exp(-\eta_L^2)\right\}\frac{d\psi_{B,m}}{d\eta_L} -k_L^2\psi_{B,m}=k_L^2\exp(-\eta_L^2)H_k(\eta_L). \tag{48b}$$

For the extreme case where $Pe\to\infty$, $R_i<<1$ but $R_i^*(=R_i\sqrt{Pe})$ has finite value, where i=A and B, Eq. (48) is reduced as

$$\left(\frac{d^2}{d\eta^2}-k^2\right)\psi_{A,m}=k^2\exp(-\eta^2)H_m(\eta), \tag{49a}$$

$$\left(\frac{d^2}{d\eta_L^2}-k_L^2\right)\psi_{B,m}=k_L^2\exp(-\eta_L^2)H_m(\eta_L), \tag{49b}$$

and can be solved analytically as

$$\psi_{A,m}=-\frac{k}{2}\left\{\exp(k\eta)\int_{\eta}^{\infty}\exp(-k\zeta-\zeta^2)H_m(\zeta)d\zeta +\exp(-k\eta)\int_{-\infty}^{\eta}\exp(k\zeta-\zeta^2)H_m(\zeta)d\zeta\right\}. \tag{50a}$$

$$\psi_{B,m}=-\frac{k_L}{2}\left\{\exp(k_L\eta_L)\int_{\eta_L}^{\infty}\exp(-k_L\zeta-\zeta^2)H_m(\zeta)d\zeta +\exp(-k_L\eta_L)\int_{-\infty}^{\eta_L}\exp(k_L\zeta-\zeta^2)H_m(\zeta)d\zeta\right\}. \tag{50b}$$

Recently, Kim [24] solved Eq. (50) analytically and suggested the following solutions:

$\psi_{A,m}=k^2(\psi_{A,m-2}+\phi_{A,m-2})$ and $\psi_{B,m}=k_L^2(\psi_{B,m-2}+\phi_{B,m-2})$, (51a & b)

for n=2, 3, 4 ⋯, with

$$\psi_{A,0}=-\frac{k}{4}\sqrt{\pi}\exp\left(\frac{k^2}{4}\right)\left[\exp(k\eta)\operatorname{erfc}\left(\eta+\frac{k}{2}\right)+\exp(-k\eta)\operatorname{erfc}\left(-\eta+\frac{k}{2}\right)\right], \quad (51c)$$

$$\psi_{B,0}=-\frac{k_L}{4}\sqrt{\pi}\exp\left(\frac{k_L^2}{4}\right)\left[\exp(k_L\eta_L)\operatorname{erfc}\left(\eta_L+\frac{k_L}{2}\right)+\exp(-k_L\eta_L)\operatorname{erfc}\left(-\eta_L+\frac{k_L}{2}\right)\right], \quad (51d)$$

and

$$\psi_{A,1}=\frac{k}{2}\exp\left(\frac{k^2}{4}\right)\left[\begin{array}{l}\exp(k\eta)\left\{\exp\left(-\left(\eta+\frac{k}{2}\right)^2\right)-\frac{k}{2}\sqrt{\pi}\operatorname{erfc}\left(\eta+\frac{k}{2}\right)\right\}+\\ \exp(-k\eta)\left\{\exp\left(-\left(\eta-\frac{k}{2}\right)^2\right)+\frac{k}{2}\sqrt{\pi}\operatorname{erfc}\left(-\eta+\frac{k}{2}\right)\right\}\end{array}\right] \quad (51e)$$

$$\psi_{B,1}=\frac{k_L}{2}\exp\left(\frac{k_L^2}{4}\right)\left[\begin{array}{l}\exp(k_L\eta_L)\left\{\exp\left(-\left(\eta_L+\frac{k_L}{2}\right)^2\right)-\frac{k_L}{2}\sqrt{\pi}\operatorname{erfc}\left(\eta_L+\frac{k_L}{2}\right)\right\}+\\ \exp(-k_L\eta)\left\{\exp\left(-\left(\eta_L-\frac{k_L}{2}\right)^2\right)+\frac{k_L}{2}\sqrt{\pi}\operatorname{erfc}\left(-\eta_L+\frac{k_L}{2}\right)\right\}\end{array}\right]. \quad (51f)$$

By applying the procedure to obtain Eq. (40), the stability equations are expressed as

$$\tau\frac{d\mathbf{C}}{d\tau}=\mathbf{F}\mathbf{C}, \quad (52a)$$

where

$$\mathbf{C}=\begin{bmatrix}\mathbf{A}\\ \mathbf{B}\end{bmatrix} \text{ and } \mathbf{F}=\begin{bmatrix}\mathbf{F}_{AA} & \mathbf{F}_{AB}\\ \mathbf{F}_{BA} & \mathbf{F}_{BB}\end{bmatrix}, \quad (52b)$$

$\mathbf{A}=[A_0, A_1, \cdots]^T$ and $\mathbf{B}=[B_0, B_1, \cdots]^T$. (52c & d)

The detailed description for the structure of the matrix **F** is given in the Appendix. Since matrix **F** is independent of τ, the growth rate σ is the maximum eigenvalue of the matrix **F**:

$$\sigma=\max\{\operatorname{eig}(\mathbf{F})\}. \quad (53)$$

2-2. Normal Mode Analysis

As discussed by Tan and Homsy [17] and Pritchard [22], one of the major differences between the present radial flow system and the rectilinear one is that the normal mode analysis is possible in the present radial fingering problem. Since the coefficients of the above Eqs. (26) and (27) are independent of τ, under the normal mode analysis, the disturbance quantities can be represented as

$$[\psi, a_1, b_1]=[\bar{\psi}(\xi), \bar{a}_1(\xi), \bar{b}_1(\xi)]\tau^{\sigma}, \quad (54)$$

where the growth rate σ defined as

$$\tau\frac{\partial X}{\partial\tau}=\sigma X, \quad (55)$$

can be used for the stability measure. From here, for the simplicity we remove bars. By substituting Eq. (54) into Eqs. (25)-(27), the following stability equations can be obtained:

$$\xi\frac{d^2\psi}{d\xi^2}+\left[1-\left(R_A\frac{da_0}{d\xi}+R_B\frac{db_0}{d\xi}\right)\xi\right]\frac{d\psi}{d\xi}-\frac{n^2}{4\xi}\psi=-\frac{n^2}{4\xi}(R_Aa_1+R_Bb_1), \quad (56)$$

$$\sigma a_1=\left[\xi\frac{\partial^2}{\partial\xi^2}+\left\{\xi+\left(1-\frac{Pe}{2}\right)\right\}\frac{\partial}{\partial\xi}-\frac{n^2}{4\xi}\right]a_1-\frac{Pe}{2}\frac{da_0}{d\xi}\psi, \quad (57)$$

$$\sigma b_1=Le^2\left[\xi_L\frac{\partial^2}{\partial\xi_L^2}+\left\{\xi_L+\left(1-\frac{Pe_L}{2}\right)\right\}\frac{\partial}{\partial\xi_L}-\frac{n^2}{4\xi_L}\right]b_1-\frac{Pe_L}{2}\frac{db_0}{d\xi_L}\psi, \quad (58)$$

under the boundary conditions (28).

For the large Pe case, from Eq. (29)-(31), the above stability equations are approximated as

$$\left\{\frac{d^2}{d\eta^2}+\left(R_A\frac{da_0}{d\eta}+R_B\frac{db_0}{d\eta}\right)-k^2\right\}\psi^*=-k^2(R_A^*a_1+R_B^*b_1), \quad (59)$$

$$2\sigma a_1=\left\{\frac{d^2}{d\eta^2}+2\eta\frac{d}{d\eta}-k^2\right\}a_1-\frac{da_0}{d\eta}\psi^*, \quad (60)$$

$$2\sigma b_1=\left\{\frac{d^2}{d\eta_L^2}+2\eta_L\frac{d}{d\eta_L}-k_L^2\right\}b_1-\frac{db_0}{d\eta_L}\frac{1}{\sqrt{Le}}\psi^*, \quad (61)$$

under the boundary conditions (32). Here $\psi^*=\sqrt{Pe}\,\psi$, $k(=n/\sqrt{Pe})$ and $R_i^*=\sqrt{Pe}\,R_i$, where i=A and B. For the extreme case of Pe→∞, Eq. (59) can be further simplified as

$$\left\{\frac{d^2}{d\eta^2}-k^2\right\}\psi^*=-k^2(R_A^*a_1+R_B^*b_1). \quad (62)$$

2-3. Numerical Shooting Method

Because the velocity disturbance field cannot be obtained analytically for the extreme case where Pe→∞ and R_i<<1, where i=A and B, a fully analytic solution is possible only for this limiting case. Therefore, the above spectral analysis has its own limit even though it can give the exact solution, and we tried to solve the stability Eqs. (56)-(58) with the numerical shooting method [25].

To integrate the stability Eqs. (56)-(58), a trial value of the eigenvalue σ and the values of $d\psi/d\xi$, a_1, $da_1/d\xi$, b_1 and $db_1/d\xi$ at ξ=Pe/2 are assumed properly for given R_A, R_B, Le, n and Pe. Since the boundary conditions (28) are all homogeneous, the value of ψ at ξ=Pe/2 can be assigned arbitrarily. This procedure is based on the shooting method in which the boundary value problem is transformed into the initial value problem. The trial values at ξ=Pe/2 give all the information to make numerical integration smoothly. The integration on the 4th-order Runge-Kutta method is performed from the displacing front, ξ=Pe/2, to the injection center, ξ=0, and to the fictitious outer boundary satisfying the infinite boundary conditions. By using the Newton-Raphson iteration, the trial values σ, $d\psi/d\xi$, a_1, $da_1/d\xi$, b_1 and $db_1/d\xi$ at ξ=Pe/2 are corrected until the

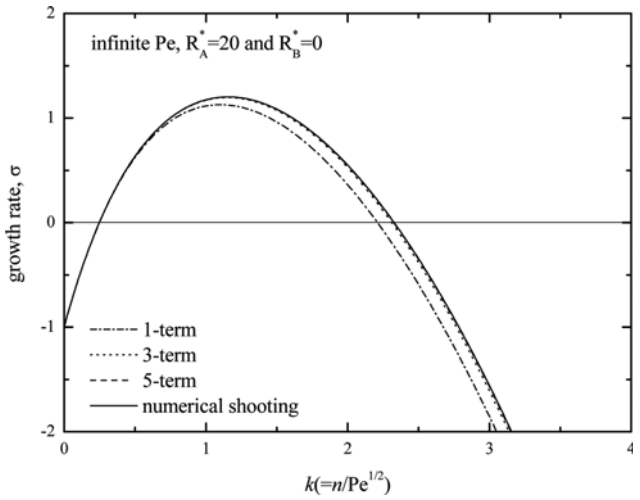

Fig. 3. Comparison of growth rates for the case of Pe=∞, R_A^*=20 and R_B^*=0.

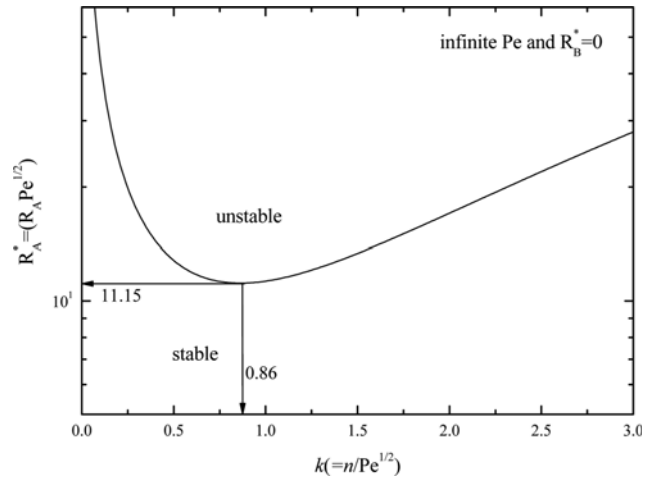

Fig. 5. Neutral stability curve under the 5-term approximation for the case of Pe=∞ and R_B^*=0.

stability equations satisfy the boundary conditions (28) within the relative tolerance of 10^{-10}. Then, by increasing the fictitious outer boundary step by step, the above integration is repeated. Finally, the value of σ is decided through the extrapolation. For the large Pe case, a similar solution procedure is applied to stability Eqs. (59)-(61).

For the limiting case of Pe→∞, R_A^*=20 and R_B^*=0, the growth rates obtained from the analytical approximations and the numerical method are compared in Fig. 3. It is interesting that the second solution is identical with the first-order one and the fifth-order solution is nearly identical with the numerical solution by using the standard shooting method.

RESULTS AND DISCUSSION

1. For the Limiting Case of Pe→∞

For the limiting case of Pe→∞, R_A→0 and R_B=0 but finite R_A^* (=$R_A\sqrt{Pe}$), based on the 5-term approximation, the analytically obtained growth rates are summarized in Fig. 3. This figure shows that there exists a critical $R_{A,c}^*$, under which the growth rate is always negative, i.e., the system is unconditionally stable. Based on the results summarized in Fig. 4 and the neutral stability curve at which σ=0 should be satisfied is calculated and featured in Fig. 5. The critical conditions determined by the minimum point of the neutral stability curve are

$$R_{A,c}^*(=R_{A,c}\sqrt{Pe})=11.15 \text{ and } k_c(=n_c/\sqrt{Pe})=0.86. \quad (63)$$

The above critical conditions mean that for a given R_A the minimum Pe from which we can expect the fingering motion is Pe_c=$126.56R_A^{-2}$ with the number of fingers n_c=$9.59R_A^{-1}$. If R_A^*>11.15, the system is unstable and the number of finger can be determined by k_{max} at which the growth rate has its maximum value for a given R_A^*.

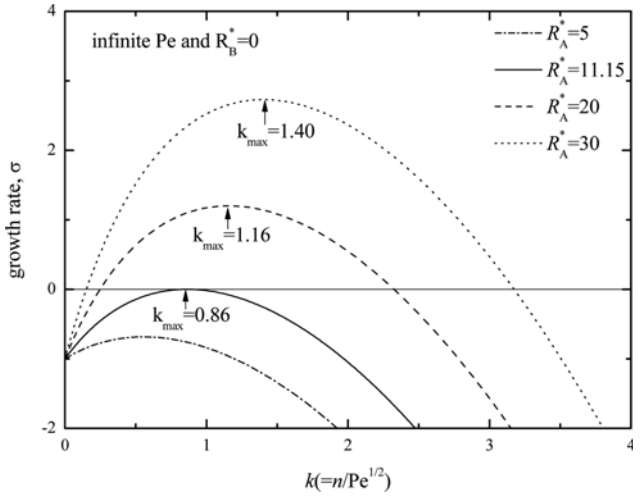

Fig. 4. Growth rates for the various R^* in the limiting case of Pe=∞ and R_B^*=0. For the region of R_A^*<$R_{A,c}^*$, the growth constant is always exponent, i.e., unconditionally stable. All results are based on the 5-term approximation.

Based on the 5-term approximation, the effect of the double diffusion on the critical condition is summarized in Fig. 6. For σ>0, the number of fingers is determined by k_{max} in which σ shows its maximum value. For the case of R_B<0, as Le increases, the system becomes stable, whereas this trend is reversed for the opposite case of R_B>0. The number of fingers at the onset condition is summarized in Fig. 6(c).

2. Finite Pe Case

Based on the spectral approach explained in section 4.1, Pritchard [22] expanded $a_1(\tau, \xi)$ and $b_1(\tau, \xi)$ as

$$a_1(\tau, \xi)=\exp(-\xi)\xi^{Pe/2}\tau^{-1}\sum_{m=0}^{\infty}A'_m(\tau)L_m^{Pe/2}(\xi), \quad (64a)$$

$$b_1(\tau, \xi)=\exp(-\xi_L)\xi_L^{Pe_L/2}\sum_{m=0}^{\infty}B'_m(\tau)L_m^{Pe_L/2}(\xi_L), \quad (64b)$$

rather than the present (37). However, this spectral expansion needs a mathematical justification for the incursion of a factor τ^{-1} and suffers from the severe singularity when τ→0. For the limiting case of n=0 and R_B=0, Pritchard [22] showed that the dominant mode of instability is

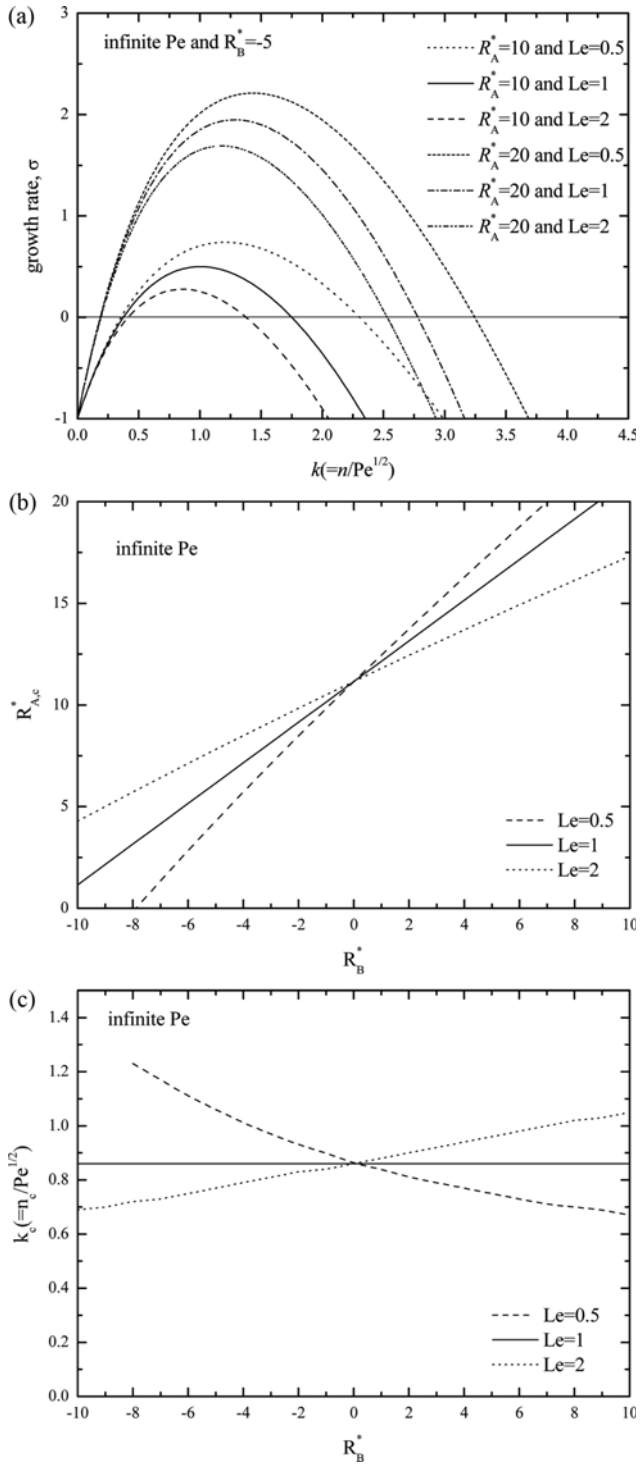

Fig. 6. Effect of Le on the (a) growth rate, (b) $R^*_{A,c}$ and (c) critical wavenumber for the limiting case of Pe=∞.

$$a_1(\tau, \xi) = A_0'(\tau)\tau^{-1}L_0^{Pe/2}(\xi)\exp(-\xi)\xi^{Pe/2}, \tag{65}$$

and the corresponding growth rate is

$$\frac{1}{A_0'}\frac{dA_0'}{d\tau} = 0 \text{ for } n = 0. \tag{66}$$

In the present definition of the growth rate, Pritchard's growth constant can be rewritten as,

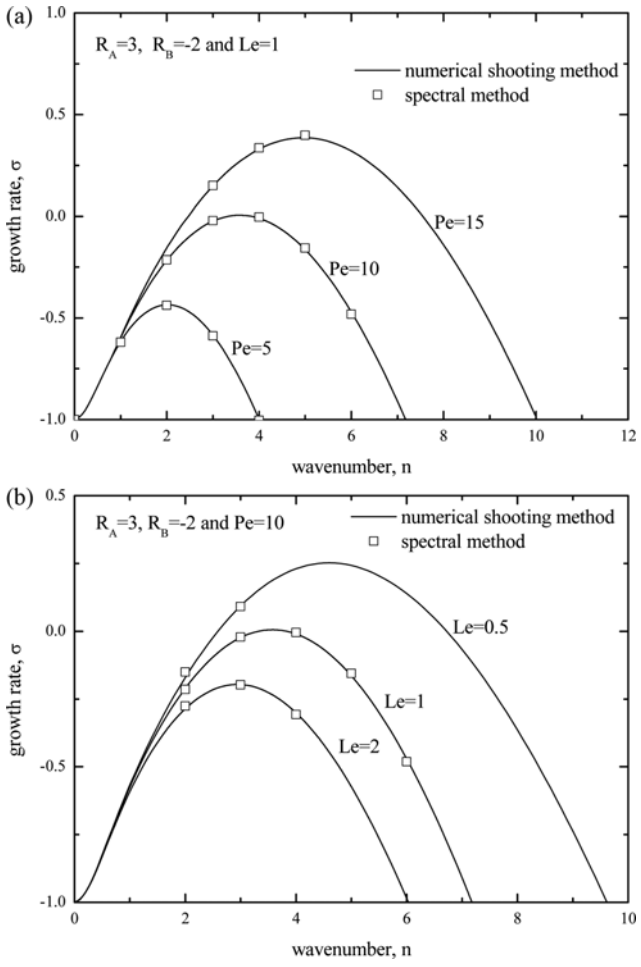

Fig. 7. Comparison of the growth rates obtained from the spectral method and the numerical shooting method. (a) Le=1 and (b) Pe=10.

$$\sigma = -1 \text{ for } n = 0, \tag{67}$$

since

$$\sigma = (1/A_0')(dA_0'/d\tau) - 1, \tag{68}$$

from Eqs. (35) and (64). As discussed by Pritchard [22], except for this limiting case of n=0, a fully analytic approach is not possible. He expanded the scalar fields using generalized Fourier series and obtained the velocity field by solving Eq. (56) numerically. We solved the stability Eqs. (56)-(58) numerically by employing the shooting method. In Fig. 7, for the example case of R_A=3 and R_B=−2, the present numerical solutions are compared with the 4-term spectral analysis results. This figure reveals that the present numerical solution and the 4-term spectral analysis support each other. For the example case of Le=2, R_A=3 and R_B=−2, the high Pe approximation is compared with the general solution in Fig. 8. Figs. 7 and 8 show that the present analytical approximations and numerical solution support each other. For the single diffusion system, Tan and Homsy [17] obtained Eq. (66) and showed that there is a critical Peclet number to insure the onset of fingering. To con-

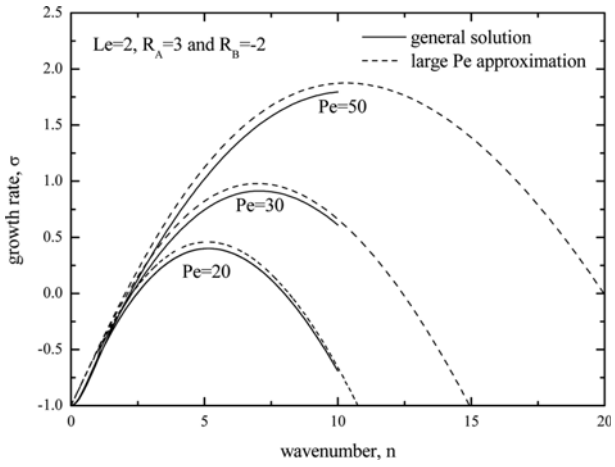

Fig. 8. Comparison of the growth rates obtained from the general solution and the large Pe approximation for the case of Le= 2, R_A=3 and R_B=−2.

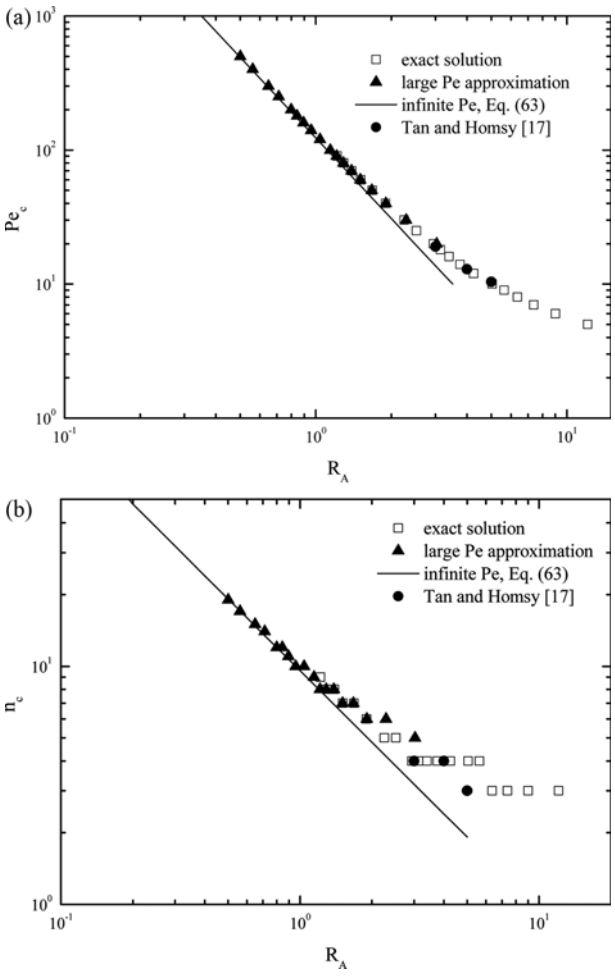

Fig. 9. Comparison of the critical conditions from the various approximations: (a) Critical Pe and (b) critical wavenumber.

firm the present solution methods, in Fig. 9, Tan and Homsy's critical conditions were compared with the present ones. As shown in this figure, the present critical conditions reproduce Tan and Homsy's.

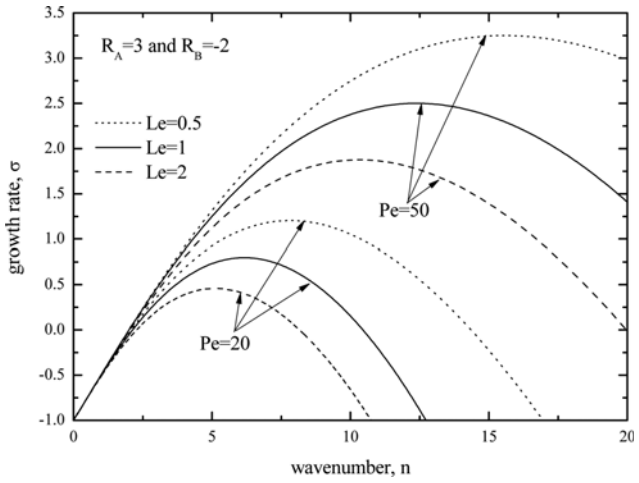

Fig. 10. Effects of Le and Pe on the growth rate for the unstable displacing and the stable displaced case.

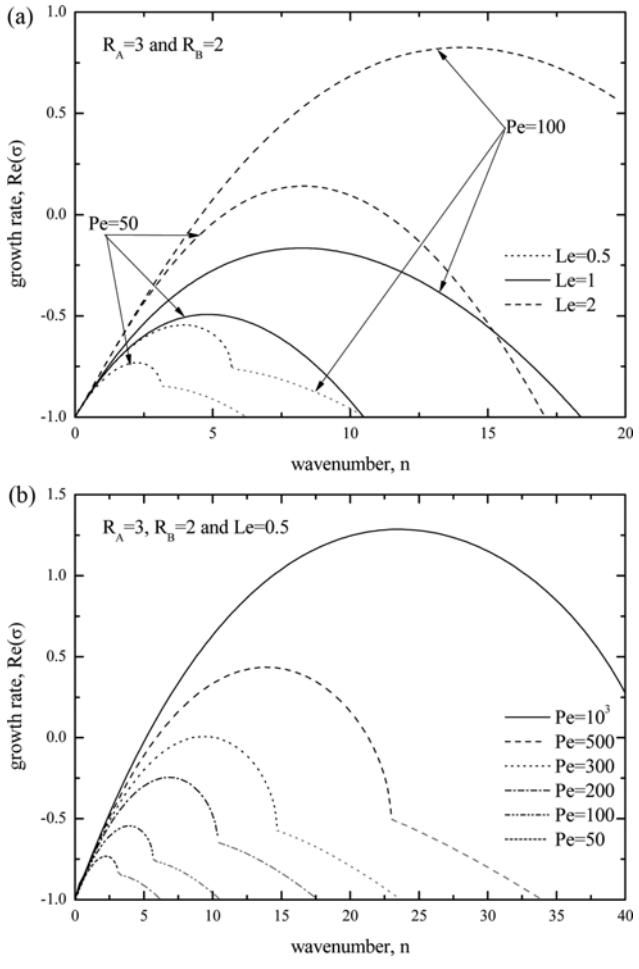

Fig. 11. Growth rate for the stable displacing and the unstable displaced case: (a) Effects of Le and Pe and (b) effect of Pe for the case of Le=0.5. Gray lines represent time-periodic oscillatory mode.

Because the present high Pe approximation explains the general solutions quite well, and real experiments correspond to the high

Pe case, from now on we use the high Pe approximation to explain the various situations. If both fluids are unstable, i.e., $R_A>0$ and $R_B<0$, the effects of Le on the growth rate of disturbance are summarized in Fig. 10. This figure shows that as Pe increases the system become unstable, whereas high Le has the effect of suppressing instability. Since the number of fingers increases with increasing Pe and decreasing Le, we can control the flow pattern by flow rate, Pe.

For the unstable displacing and the stable displaced phases, i.e. $R_A>0$ and $R_B>0$, the effect of Pe and Le on the stability characteristics is given in Fig. 11. In this regime, the time periodic instability, $\mathrm{Im}(\sigma)\neq0$, is more unstable than the stationary one, $\mathrm{Im}(\sigma)=0$, for the case of Le<1 and higher wavenumber. However, since the most unstable mode is the stationary one, as shown in Figs. 11(a) and (b), we cannot expect the time periodic oscillatory mode in real experiments. In this case, high Le has the effect of making the system unstable, i.e., accelerates the growth of instabilities.

For the stable displacing and the unstable displaced phases, $R_A<0$ and $R_B<0$, the time periodic instability is more unstable than the stationary one, for the case of Le>1 and higher wavenumber, as shown in Figs. 12(a) and (b). However, like the case of $R_A>0$ and $R_B>0$, we cannot expect a time periodic oscillatory mode in real experiments. In this case, high Le has the effect of making the system stable, i.e., suppresses the growth of instabilities.

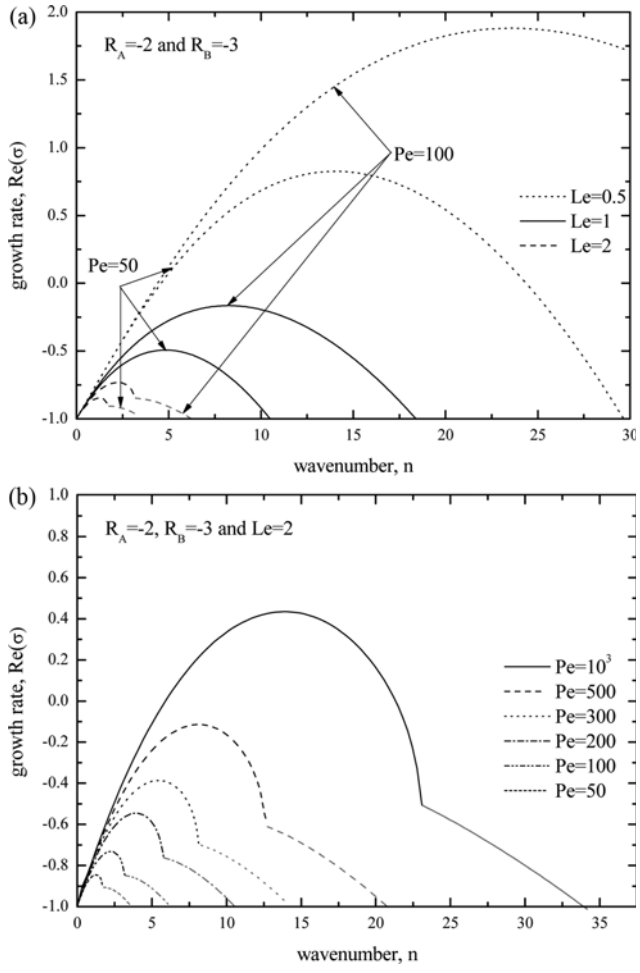

Fig. 12. Growth rate for the unstable displacing and the stable displaced case: (a) Effects of Le and Pe and (b) effect of Pe for the case of Le=2. Gray lines represent time-periodic oscillatory mode.

CONCLUSIONS

The effects of double diffusion on the growth of radial viscous fingering in a porous medium or a Hele-Shaw cell were analyzed under linear stability theory. In the self-similar domain, the stability equations were derived under the normal mode analysis and solved analytically and numerically. For the limiting case of very high Pe, the disturbances were expanded as a series of orthogonal functions and the growth rate was obtained analytically by solving matrix eigenvalue problem. Also, for small Pe system, the growth rates obtained analytically support the numerical shooting solutions. For the case of Pe≥20, the stability characteristics obtained under the large Pe approximation explain the system reasonably well.

In the present system, as expected, high Pe has the effect of making the system unstable, i.e., accelerates the growth of instabilities, regardless of the magnitude of Le. The effect of Le on the growth of the instabilities is strongly dependent on the viscosity distribution. If the displaced phase is stable, i.e., $R_B>0$, Le makes the system unstable, regardless of Pe, whereas, for the case of $R_B<0$, i.e., the displaced phase is unstable, the effect of Le on the growth of the instabilities is reversed.

ACKNOWLEDGEMENT

This research was supported by the 2017 scientific promotion program funded by Jeju National University.

REFERENCES

1. S. Hill, *Chem. Eng. Sci.*, **1**, 247 (1952).
2. R. L. Slobod and R. A. Thomas, *Soc. Pet. Eng. J.*, **3**, 9 (1963).
3. T. E. Perkins, O. E. Johnston and R. N. Hoffman, *Soc. Pet. Eng. J.*, **5**, 301 (1965).
4. C. T. Tan and G. M. Homsy, *Phys. Fluids*, **29**, 3549 (1986).
5. G. M. Homsy, *Ann. Rev. Fluid Mech.*, **19**, 271 (1987).
6. A. De Wit, Y. Bertho and M. Martin, *Phys. Fluids*, **17**, 054114 (2005).
7. G. Rousseaux, A. De Wit and M. Martin, *J. Chromatogr. A*, **1149**, 254 (2007).
8. Y. Nagatsu, Y. Ishii, Y. Tada and A. De Wit, *Phys. Rev. Lett.*, **113**, 024502 (2014).
9. F. Haudin, J. H. E. Cartwright, F. Brau and A. De Wit, *PNAS*, **111**, 17363 (2014).
10. F. Haudin and A. De Wit, *Phys. Fluids*, **27**, 113101 (2015).
11. G. Schuszter and A. De Wit, *J. Chem. Phys.*, **145**, 224201 (2016).
12. G. Schuszter, F. Brau and A. De Wit, *Phys. Chem. Chem. Phys.*, **18**, 25592 (2016).
13. F. Brau, G. Schuszter and A. De Wit, *Phys. Rev. Lett.*, **118**, 134101 (2017).
14. D. Pritchard, *Eur. J. Mech. B/Fluids*, **28**, 564 (2009).
15. M. Mishra, P. M. J. Trevelyan, C. Almarcha and A. De Wit, *Phys. Rev. Lett.*, **105**, 204501 (2010).

16. J. Azaiez and M. Sajjadi, *Phys. Rev. E*, **85**, 026306 (2012).
17. C. T. Tan and G. M. Homsy, *Phys. Fluids*, **30**, 1239 (1987).
18. Y. C. Yortsos, *Phys. Fluids*, **30**, 2928 (1987).
19. A. Riaz and E. Meiburg, *Phys. Fluids*, **15**, 938 (2003).
20. A. Riaz and E. Meiburg, *J. Fluid Mech.*, **494**, 95 (2003).
21. A. Riaz, C. Pankiewitz and E. Meiburg, *Phys. Fluids*, **16**, 3592 (2004).
22. D. Pritchard, *J. Fluid Mech.*, **508**, 133 (2004).
23. M. Abramowitz and I. A. Stegun, Handbook of Mathematical Functions with Formulas, Graphs, and Mathematical Tables, New York, Dover Publications (1972).
24. M. C. Kim, *Transp. Porous Med.*, **97**, 395 (2013).
25. M. C. Kim, *Korean J. Chem. Eng.*, **34**, 189 (2017).

APPENDIX

The matrices in Eq. (40) are given by

$$[\mathbf{D}_{AA}]_{i,j}=\int_0^\infty \exp(-\xi)\xi^{Pe/2}\phi_{A,j-1}\left\{L_A-\frac{n^2}{4\xi}\right\}\phi_{A,i-1}d\zeta - \frac{Pe}{2}R_A\int_0^\infty \frac{da_0}{d\xi}\exp(-\xi)\xi^{Pe/2}\phi_{A,j}\psi_{A,i}d\xi = -\lambda_{i-1}\delta_{i-1,j-1}-\frac{n^2}{4}\alpha_i\alpha_j\sum_{l=0}^{i\le j}\Gamma(l+Pe/2+1)/\Gamma(l+1) - \frac{Pe}{2}R_A\int_0^\infty \frac{da_0}{d\xi}\exp(-\xi)\xi^{Pe/2}\phi_{A,j}\psi_{A,i}d\xi \quad (A1)$$

$$[\mathbf{D}_{AB}]_{i,j}=-\frac{Pe}{2}R_B\int_0^\infty \frac{da_0}{d\xi}\exp(-\xi)\xi^{Pe/2}\phi_{A,j}\psi_{B,i}d\xi, \quad (A2)$$

$$[\mathbf{D}_{BA}]_{i,j}=-\frac{Pe}{2}R_A\int_0^\infty \exp(-\xi_L)\xi_L^{Pe_L/2}\frac{db_0}{d\xi_L}\phi_{B,j-1}\psi_{A,i-1}d\xi_L, \quad (A3)$$

$$[\mathbf{D}_{BB}]_{i,j}=\int_0^\infty \exp(-\xi_L)\xi_L^{Pe_L/2}\phi_{B,j-1}\left\{L_B-\frac{n^2}{4\xi_L}\right\}\phi_{B,i-1}d\xi_L - \frac{Pe}{2}R_B\int_0^\infty \frac{db_0}{d\xi_L}\exp(-\xi_L)\xi_L^{Pe_L/2}\phi_{B,j-1}\psi_{T,i}d\xi_L = -\lambda_{i-1}\delta_{i-1,j-1}-\frac{n^2}{4}\beta_i\beta_j\sum_{l=0}^{i\le j}\Gamma(l+Pe_L/2+1)/\Gamma(l+1) - \frac{Pe}{2}R_B\int_0^\infty \frac{db_0}{d\xi_L}\exp(-\xi_L)\xi_L^{Pe_L/2}\phi_{B,j-1}\psi_{T,i}d\xi_L \quad (A4)$$

where i=1, 2, ⋯, N+1 and j=1, 2, ⋯, N+1.

For the limiting case of Pe→∞, the above matrices are reduced as (see Eq. (52)).

$$[\mathbf{F}_{AA}]_{i,j}=\frac{1}{2}\int_{-\infty}^\infty \exp(\zeta^2)\phi_{A,j-1}\left(\frac{\partial^2}{\partial\zeta^2}+2\zeta\frac{\partial}{\partial\zeta}-k^2\right)\phi_{A,i-1}d\zeta + \frac{k^2}{2\sqrt{\pi}}R_A^*\int_{-\infty}^\infty \phi_{A,j}\psi_{A,i}d\zeta = -\frac{1}{2}(A_{i-1}+k^2)\delta_{i-1,j-1}+\frac{k^2}{2\sqrt{\pi}}R_A^*\int_{-\infty}^\infty \phi_{C,j}\psi_{C,i}d\zeta \quad (A5)$$

$$[\mathbf{F}_{AB}]_{i,j}=\frac{a^2}{2\sqrt{\pi}}R_B^*\int_{-\infty}^\infty \phi_{A,j-1}\psi_{B,i-1}d\zeta, \quad (A6)$$

$$[\mathbf{F}_{BA}]_{i,j}=\frac{k^2}{2\sqrt{Le\pi}}R_A^*\int_{-\infty}^\infty \phi_{B,j-1}\psi_{A,i-1}d\zeta, \quad (A7)$$

$$[\mathbf{F}_{BB}]_{i,j}=\frac{1}{2}\int_{-\infty}^\infty \exp(\zeta_L^2)\phi_{T,j-1}\left(\frac{\partial^2}{\partial\zeta_L^2}+2\zeta_L\frac{\partial}{\partial\zeta_L}-k_L^2\right)\phi_{B,i-1}d\zeta_L + \frac{k_L^2}{2\sqrt{Le\pi}}R_T^*\int_{-\infty}^\infty \phi_{T,j-1}\psi_{T,i-1}d\zeta_L = -\frac{1}{2}(\lambda_{i-1}+k_L^2)\delta_{i-1,j-1}+\frac{k^2}{2\sqrt{Le\pi}}R_B^*\int_{-\infty}^\infty \phi_{T,j-1}\psi_{T,i-1}d\zeta_L \quad (A8)$$